

# Experimental Model Design for Oilwell Drilling Rig Circulation System Studies Part III. (computational modeling and similarity of the test rig)

*Mohamed Milad Ahmed*  
*e-mail: massiwi@su.edu.ly*

*Department of Petroleum, Faculty of Engineering, Sirte University (SU), Libya*

## Abstract

This paper is the third in a series of an experimental apparatus design for annular flow studies. Earlier articles considered the preliminary design of the experimental rig, in terms of preliminary scaling from field data, dimensional analysis and design and suggested experimental conditions, the rig design constrains, rig parameters, and rig construction were considered in part II. In order for to the experimental apparatus to be valid to simulate actual field dimensions and flow parameters a scaling symmetry and similarity between experimental and field data were considered in the present paper (part III), normalized local axial velocity with the inlet velocity against normalized local radius with the radius of the pipe for both experimental and field data were plotted and superimposed, the results showed that both cases were coincides, this implies that the experimental rig is verified and valid for running experiments.

## 1. Introduction

Flow through annulus may experience different geometries such as sudden reduction in inner wall such as changes in diameter of drill pipes and sudden expansion such as change in diameters between open and cased hole as fluid flows up the annuals and, the more complex geometry such that found inside and around the drilling bit.

As a first step towards building understanding of these complex flows, this study is intended to experimentally and computationally investigate incompressible Newtonian fluid flow behaviour in terms of axial and tangential velocities through the annulus of vertical uniform concentric pipes,

with rotation of the inner pipe. The computational work was based on commercially available CFD software (Fluent)[1], typical of that likely to be used in industry, this study will be carried out in parts, the general strategy was to start with a simple geometry consisting of uniform vertical concentric pipes with and without rotation of the inner pipe carrying single phase working fluid (without solids). Future study could move on to more complicated geometries, such as sudden expansion of the outer pipes and expansion or contraction of the inner pipes, with and without solids carried by the flow and, eventually, to model the most difficult flow at the rotating drilling bit itself. In this paper a physical experimental model of uniform vertical concentric pipes with rotation of the inner pipe was designed with dimensions scaled from real dimensions of actual oil well. The geometry of the model was investigated by Fluent to check validity of the model, were the results were very acceptable.

There are various drilling problems may encountered while drilling gas and oil well due to poor hole cleaning (lifting solids) related to drilling fluid properties and flow behavior, such as slow drilling rates or excessive drill pipe torque. Some merely render the drilling less efficient. Others, such as a stuck drill pipe or loss of circulation, interrupt the drilling progress for weeks which raises the cost and loss time of drilling and sometimes leads to abandonment of the well[2] and [3]. The problem becomes more critical during drilling of directional and horizontal wells, due to the hole inclination and tendency of the drilled cuttings to accumulate in the lower side of the hole.

Drilling fluid properties and flow behavior are key factors in avoiding such problems[2],[3]and [4] . This study is aimed at finding optimum flow and drilling fluid properties to be used in a typical offshore oil field such as Bouri, Libya[5]. Computational Fluid Dynamics (CFD) is potentially a powerful tool for achieving these objectives, but the first step is to verify that it can be applied successfully to the problem. The study will compare experimental velocities measured using a Laser Doppler Velocimeter (LDV) [6] and [7] technique with model simulations using CFD software. This paper as a first part of the study will consider the preliminary design of a physical experimental model.

## 2. experimental apparatus

The experimental apparatus used should be:

Easy to construct and operate.

1. Able to provide clearly defined boundary conditions for comparison with CFD codes.
2. Representative of field flows, ie be scaled to operate at similar Reynolds and swirl numbers
3. Able to allow detailed LDV measurements of flow properties in the annular flow region between well casing and drilling string.
4. Sufficiently simple to focus comparison on modeling of only swirling developing flow.

### CFD MODELING OF THE PROPOSED EXPERIMENTAL FLOW

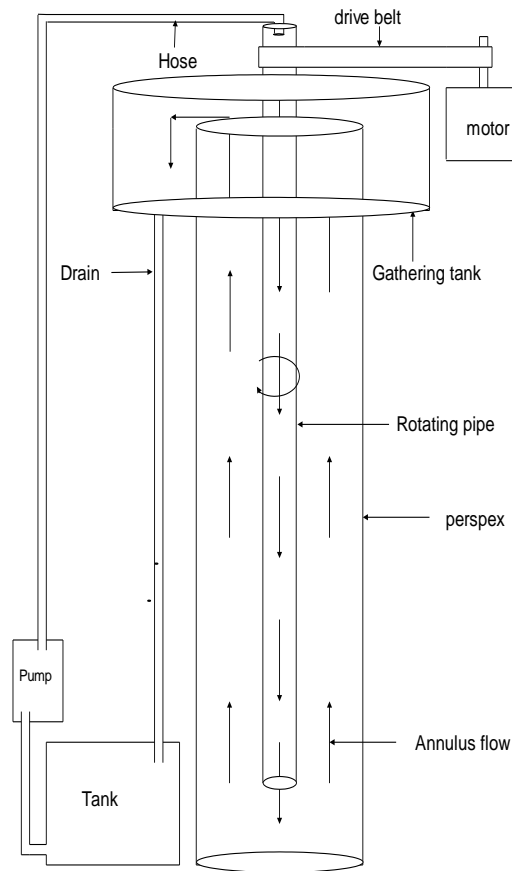


**Figure 1** Physical experimental model.

Fig 1 indicates the proposed experimental model. One obvious problem will be the “whipping” of the lower end of the rotating pipe due to pipe straightness and support bearing tolerance. If every

effort is made to minimize these, and the flow measurements are taken higher up the apparatus nearer to the support bearings, then it will be assumed that this has negligible influence on the measured velocities. Therefore in computational model, any “whipping” will be ignored.

A computational model for the dimensions as calculated in part I [8] shown in Table 1 was created. Fig 2 shows the boundary types and boundary conditions of the model with the rack lines specified at different distances off the bottom of the model. The model was created, the necessary grids produced, and the necessary boundary types were specified using the pre-processor (Gambit) supplied by Fluent Inc. (Fluent Inc. 2001) [1]. The outlet condition is open to atmosphere. Accordingly the outlet boundary condition is radial equilibrium pressure and zero gauge pressure. The model was then exported to a finite volume method based CFD solver (Fluent Inc 2001). Two turbulence modeling methods were used, which were the  $k-\varepsilon$  and RSM methods. Grid independence was tested by reducing the grid size of the model by 30% from the original grid size, where all other aspects were kept without change. The results obtained show no crucial difference of the axial velocity plots for either the flow in the rotating pipe (-ve velocities) or the flow in the annulus (+ve velocities), as shown in Fig 3.

**Table 1** Experimental and field variables with typical values required for annular modeling.

Variable	Symbol	Experimental Value	Field Value
Drilling fluid flow rate	Q	$2.45 \times 10^{-3} \text{ m}^3/\text{s}$	$43.2 \times 10^{-3} \text{ m}^3/\text{s}$
Drilling fluid density	$\rho$	$1000 \text{ kg}/\text{m}^3$	$1440 \text{ kg}/\text{m}^3$
Drilling viscosity	$\nu$	$10^{-6} \text{ m}^2/\text{s}$	$8.5 \times 10^{-6} \text{ m}^2/\text{s}$
Hole diameter	D	150 mm	311.2 mm
Drill pipe external diameter	$d_e$	61.2 mm	127 mm
Drill pipe internal diameter	$d_i$	36.74 mm	76.2 mm
Drill pipe thickness	T	12.23 mm	25.4 mm
Bottom hole drill pipe clearance	C	147 mm	304.8 mm
Drill pipe rotation speed	$\Omega$	4.6 rad/s	9 rad/s

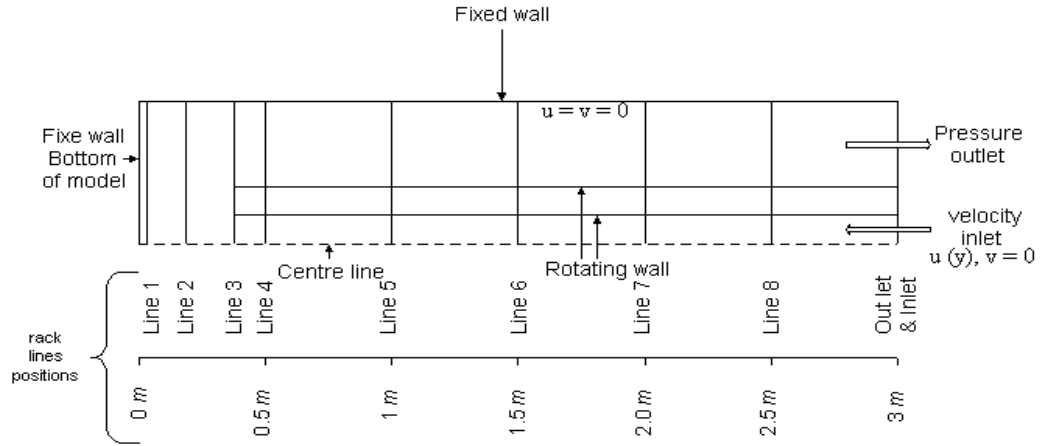


**Figure 2** Model geometry with the boundary types and boundary conditions. Rack lines are located at specific distances off the bottom of the model.

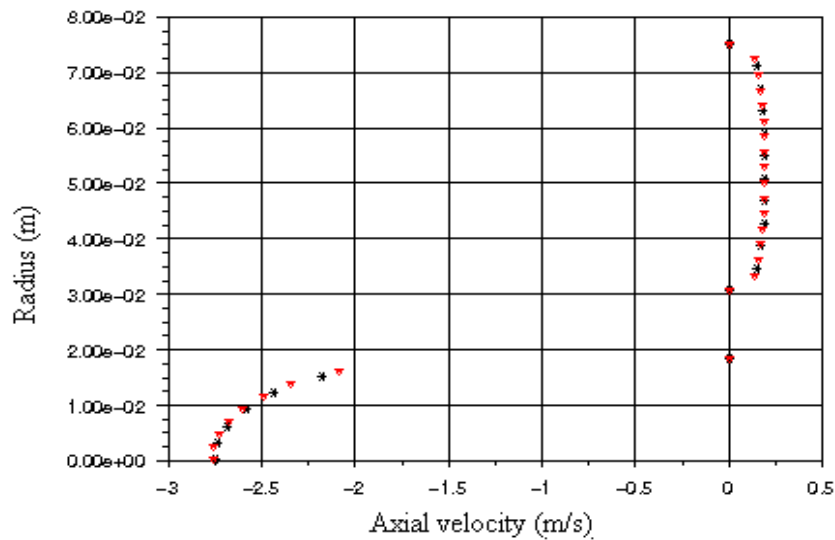


**Figure 3** Grid size effect on axial velocity profile at rack line 6 using  $k-\epsilon$  model  
 \* 30 % off grid size  
 ▼ original grid size

Display of axial velocity at specific rack lines pre-specified at a particular distances off the model bottom, reveal the shape of the velocity profile for turbulent flow. Fig 4 shows the axial velocity profile at rack lines 4 to 8 located at 0.5 m, 1.0 m, 1.5 m, 2.0 m, 2.5 m off the bottom of the model,

and at inlet and outlet. The axial velocity is clearly fully developed at line 6, 1.5 m off the model bottom.

Regarding the output obtained using initial and boundary conditions of the adopted model shown in Fig 2, the axial velocity is clearly fully developed at line 6 located 1.5 m off the bottom of the model that represents the half length of the model of a total length of 3 m, so a physical model of 2 m length would be long enough. According to this an inner pipe length of 2.245 m is adequate. There is a physical restriction on the overall height of the model if the overhead crane facilities in the laboratory are to be used.

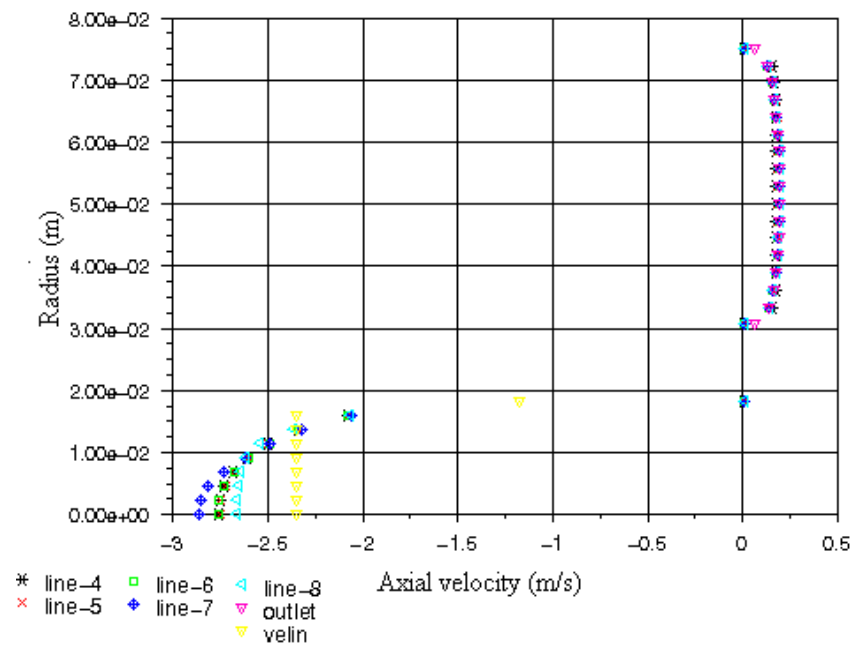


**Figure 4** Axial velocity profile at lines 4 to 8 and outlet and inlet ( $k-\epsilon$  modeling method)

The reduced model was therefore rebuilt using a reduced model length of  $L = 10D = 1.5$  m. The results in Fig 5 show no difference. This shows that it will be reasonable to build a more practical physical experimental model with a shorter length of 1.5 m. instead of 3 m.

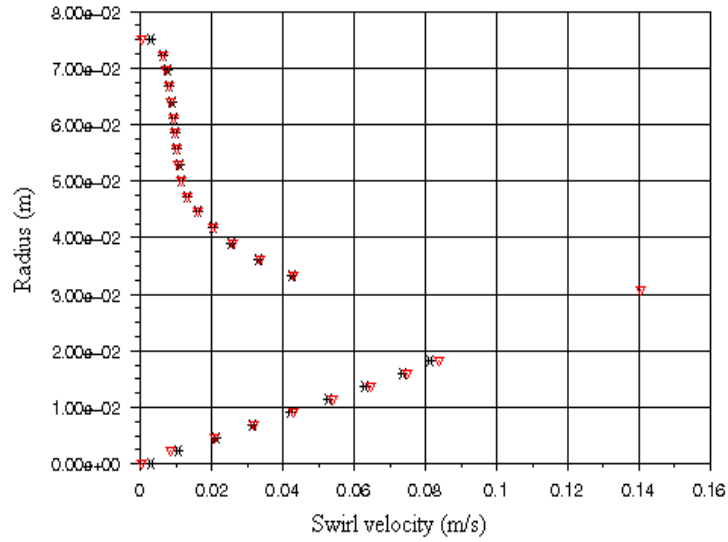


**Figure 5** Model length effect on swirl velocity ( $k-\varepsilon$  modeling method) at rack line 5

- \* Model length = 10D
- ▼ Model length = 20D

By comparing the results of the two turbulence model methods, some differences mainly appear in the radial and swirl velocity components, which are clear in the annulus (outflow) at all rack lines, Fig6 and 7. As radial velocities are very small, this indicate that the ability to measure the swirl velocity component with the LDV will be a crucial feature of the experiment if it is to discriminate between turbulence methods.

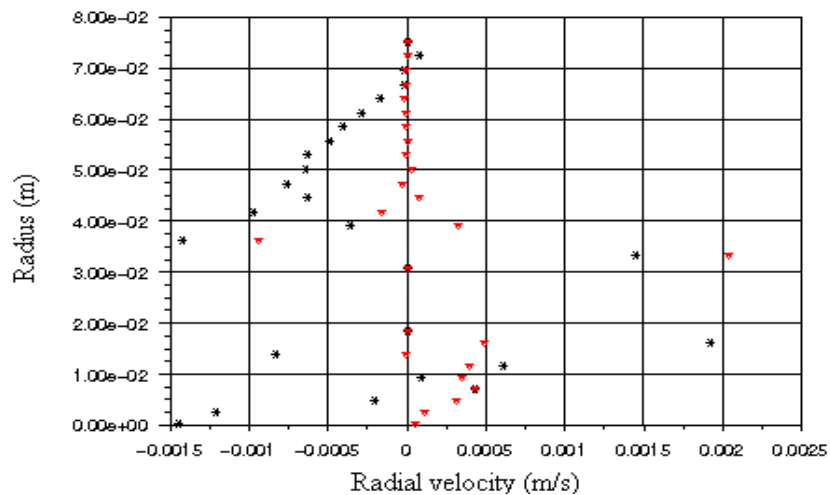


**Figure 6** Radial velocity profile for the two modeling methods  $k-\varepsilon$  and RSM, at a rack line 1.5 m off the bottom of the model

\* RSM model  
 ▼  $k-\varepsilon$  model

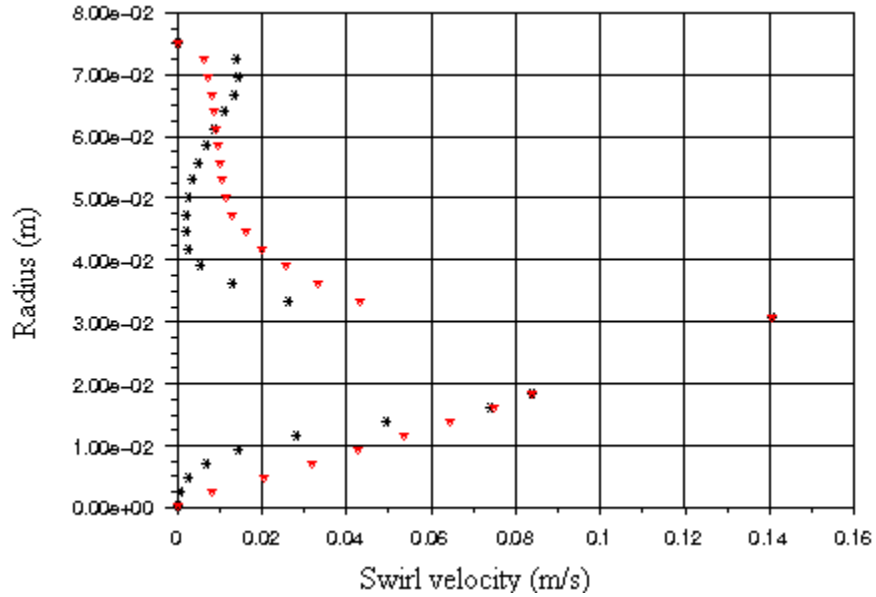


**Figure 7** Swirl velocity profile for the two modelling methods  $k-\varepsilon$  and RSM, at a rack line 1.5m off the bottom of the model

\* RSM model  
 ▼  $k-\varepsilon$  model

### 3. SCALING SYMMETRY AND SIMILARITY CONFIRMATIONS

From part one of this series[8] the experimental and field variables with their typical values were collected, summarized and tabulated as shown in table 1 above.

To verify the similarity between experimental and field data in terms of scaling and operating parameters, a plot of normalized local axial velocity with the inlet velocity  $\frac{U(r)}{|U_{inlet}|}$ , against

normalized local radius with the radius of the pipe  $\frac{r(y)}{R}$  for both experimental and field dimensions should be performed.

Inlet velocity for inflow pipe for experimental and field data can be calculated by taking advantages of the data shown in Table 1 above.

By virtue of continuity equation, the inlet velocity for inflow pipe for experimental data is as following:

$$\begin{aligned} Q_{\text{inlet}} &= A_{\text{inlet}} \times U_{\text{inlet}} \rightarrow U_{\text{inlet}} = Q_{\text{inlet}} / A_{\text{inlet}} \\ U_{\text{inlet}} &= Q_{\text{inlet}} / ((\pi/4) \times D^2) \\ &= 2.45 \times 10^{-3} / ((\pi/4) \times (36.74 \times 10^{-3})^2) \\ &= 2.45 \times 10^{-3} / 0.00106 = 2.31 \text{ m/s} \end{aligned}$$

Where,  $U_{\text{inlet}}$  = Inlet flow velocity (m/s)

$A_{\text{inlet}}$  = Inlet pipe area in ( $m^2$ )

$Q_{\text{inlet}}$  = Inlet volumetric flow rate in ( $m^3/s$ )

Similarly inlet velocity for field data is as following:

$$\begin{aligned} Q_{\text{inlet}} &= A_{\text{inlet}} \times U_{\text{inlet}} \rightarrow U_{\text{inlet}} = Q_{\text{inlet}} / A_{\text{inlet}} \\ U_{\text{inlet}} &= Q / ((\pi/4) \times D^2) \\ &= 43.2 \times 10^{-3} / ((\pi/4) \times (76.2 \times 10^{-3})^2) \\ &= 43.2 \times 10^{-3} / 0.00456 = 9.47 \text{ m/s} \end{aligned}$$

The local inlet velocities which are function in the distance away from the wall  $U(r)$  were obtained from the computationally plot of local velocity against distance (across pipe radius)  $r(y)$  for experimental and field data using the model geometry with the boundary types and boundary conditions as show in Fig. 2.

Tables 2 to 5 show the relationship between ratio of local velocity to absolute inlet velocity  $\frac{U(r)}{|U_{inlet}|}$  and ratio of local radius to pipe radius  $\frac{r(y)}{R}$  for both experimental and field data. Fig 8 shows the plots of these data are very similar.

**Table 2** Axial velocity data in inflow pipe (experimental dimensions).

$\frac{r(y)}{R}$	$\frac{0}{0.075}$ = 0	$\frac{0.005}{0.075}$ = 0.070	$\frac{0.01}{0.075}$ = 0.133	$\frac{0.015}{0.075}$ = 0.2	$\frac{0.0182}{0.075}$ = 0.243
$\frac{U(r)}{ U_{inlet} }$	$\frac{-2.75}{ 2.31 }$ = -1.19	$\frac{-2.70}{ 2.31 }$ = -1.17	$\frac{-2.60}{ 2.31 }$ = -1.13	$\frac{-2.3}{ 2.31 }$ = -0.99	$\frac{0}{ 2.31 }$ = 0

**Table 3** Axial velocity data in annulus (experimental dimensions).

$\frac{r(y)}{R}$	$\frac{0.0305}{0.075}$ = 0.41	$\frac{0.035}{0.075}$ = 0.47	$\frac{0.04}{0.075}$ = 0.53	$\frac{0.045}{0.075}$ = 0.6	$\frac{0.05}{0.075}$ = 0.67	$\frac{0.055}{0.075}$ = 0.73	$\frac{0.06}{0.075}$ = 0.8	$\frac{0.065}{0.075}$ = 0.866	$\frac{0.07}{0.075}$ = 0.933	$\frac{0.075}{0.075}$ = 1
$\frac{U(r)}{ U_{inlet} }$	$\frac{0}{ 2.31 }$ = 0	$\frac{0.130}{ 2.31 }$ = 0.056	$\frac{0.18}{ 2.31 }$ = 0.078	$\frac{0.19}{ 2.31 }$ = 0.082	$\frac{0.195}{ 2.31 }$ = 0.084	$\frac{0.19}{ 2.31 }$ = 0.082	$\frac{0.18}{ 2.31 }$ = 0.078	$\frac{0.175}{ 2.31 }$ = 0.076	$\frac{0.165}{ 2.31 }$ = 0.071	$\frac{0}{ 2.31 }$ = 0

**Table 4** Axial velocity data in inflow pipe (field dimensions).

$\frac{r(y)}{R}$	$\frac{0}{0.1556}$ = 0	$\frac{0.01}{0.1556}$ = 0.064	$\frac{0.02}{0.1556}$ = 0.13	$\frac{0.03}{0.1556}$ = 0.2	$\frac{0.0381}{0.1556}$ = 0.245
$\frac{U(r)}{ U_{inlet} }$	$\frac{-11}{ 9.47 }$ = -1.16	$\frac{-10.9}{ 9.47 }$ = -1.15	$\frac{-10.5}{ 9.47 }$ = -1.11	$\frac{-9.3}{ 9.47 }$ = -0.98	$\frac{0}{ 9.47 }$ = 0

**Table 5** Axial velocity data in annulus (field dimensions).

$\frac{r(y)}{R}$	$\frac{0.0635}{0.1556}$ = 0.41	$\frac{0.07}{0.1556}$ = 0.45	$\frac{0.08}{0.1556}$ = 0.51	$\frac{0.09}{0.1556}$ = 0.58	$\frac{0.10}{0.1556}$ = 0.64	$\frac{0.11}{0.1556}$ = 0.71	$\frac{0.125}{0.1556}$ = 0.8	$\frac{0.14}{0.1556}$ = 0.9	$\frac{0.15}{0.1556}$ = 0.96	$\frac{0.1556}{0.1556}$ = 1
$\frac{U(r)}{ U_{inlet} }$	$\frac{0}{ 9.47 }$ = 0	$\frac{0.5}{ 9.47 }$ = 0.053	$\frac{0.07}{ 9.47 }$ = 0.074	$\frac{0.07}{ 9.47 }$ = 0.074	$\frac{0.075}{ 9.47 }$ = 0.079	$\frac{0.075}{ 9.47 }$ = 0.079	$\frac{0.075}{ 9.47 }$ = 0.079	$\frac{0.07}{ 9.47 }$ = 0.074	$\frac{0.5}{ 9.47 }$ = 0.053	$\frac{0}{ 9.47 }$ = 0

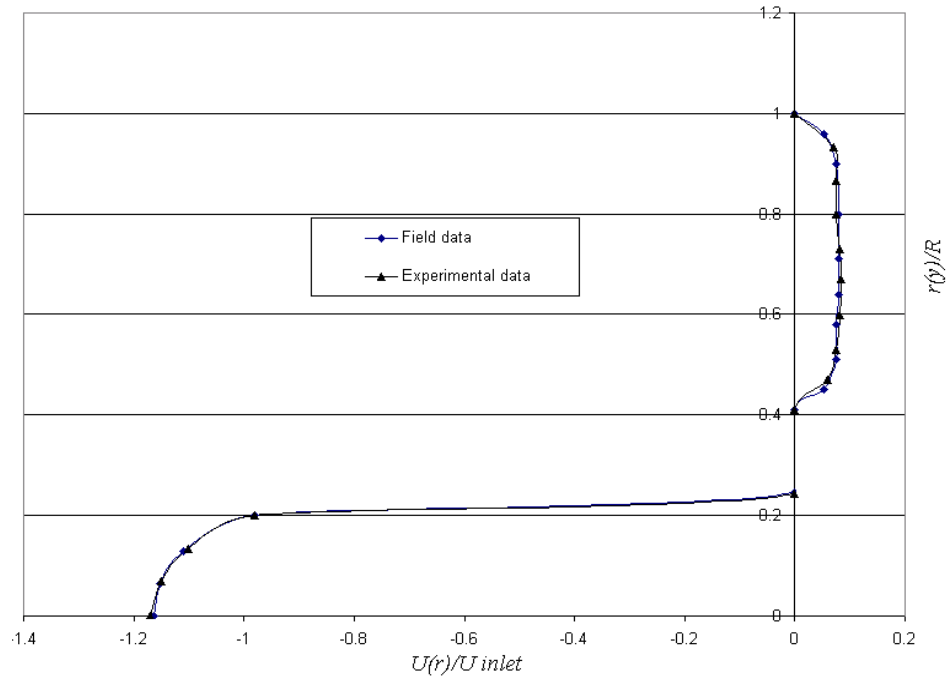


**Figure 8** Plot of experimental data against field data.

**Conclusions:**

- i. The physical model Fig 1 gives a crucial difference of radial and swirling velocity profiles as shown in Fig 6 and Fig 7 respectively for all CFD codes used which were RSM and k-ε. This will enable us comparison with the physical results.

- ii. Dimensional analysis demonstrated in part I helps to specify experimental rig diameter ratios and axial and swirl Reynolds Numbers to ensure geometric and dynamic similarity of the test rig to field conditions (Fig 8).
- iii. It was demonstrated that the proposed dimensionless groups provided in part I did give appropriate scaling (Fig 8).
- iv. A rig configuration minimised the impact of the user-specified inflow and outflow boundary conditions.
- v. Literature suggests comparison of  $k-\epsilon$  and RSM.
- vi. Preliminary CFD studies aid in physical design
  - confirms suitable model length
  - identifies importance of measuring swirl flow

## References

---

- [1]. Fluent Inc. (2001). Fluent 6.0 Users Guide, Dec. 2001. 5 Vols, Fluent Inc, Lebanon NH, USA.
- [2]. George R. Gray and Darley, H.C.H. (1980). Composition and Properties of Oil Well Drilling Fluids, Fourth Edition, Gulf Publishing Company, Houston.
- [3]. Rabia, H. (1985). Oil Well Drilling Engineering: Principles and Practice. Graham & Trotman Ltd, London.
- [4]. Preston L. Moore (1986). Drilling Practices Manual, Tulsa, Oklahoma USA.
- [5]. Agip Oil Company, L. B., S.P.L.A.J., (1992). Bouri Field Development. Tripoli.
- [6]. Durrani, T. S. and C. A. Greated (1977). Laser Systems in Flow Measurement. Plenum Press, New York.
- [7]. Durst, F. et al (1981). Principles and Practice of Laser-Doppler Anemometry. Academic Press Inc, London.
- [8]. Ahmed, M. M. (2016). Experimental Model Design For Oilwell Drilling Rig Circulation System Studies Part I. Sirte University scientific journal, volume 6, Issue 2, PP 01-14